LETTER

Corrected: Author Correction

https://doi.org/10.1038/s41586-019-1311-3

Distinct modes of mitochondrial metabolism uncouple T cell differentiation and function

Will Bailis[1,2,12], Justin A. Shyer[1,12], Jun Zhao[1,3,4], Juan Carlos Garcia Canaveras[5,6,7], Fatimah J. Al Khazal[8], Rihao Qu[1,3,4], Holly R. Steach[1], Piotr Bielecki[1], Omair Khan[1], Ruaidhri Jackson[1], Yuval Kluger[3,4,9], Louis J. Maher III[8], Joshua Rabinowitz[5,6,7], Joe Craft[1,10]* & Richard A. Flavell[1,11]*

Activated CD4 T cells proliferate rapidly and remodel epigenetically before exiting the cell cycle and engaging acquired effector functions. Metabolic reprogramming from the naive state is required throughout these phases of activation[1]. In CD4 T cells, T-cell-receptor ligation—along with co-stimulatory and cytokine signals—induces a glycolytic anabolic program that is required for biomass generation, rapid proliferation and effector function[2]. CD4 T cell differentiation (proliferation and epigenetic remodelling) and function are orchestrated coordinately by signal transduction and transcriptional remodelling. However, it remains unclear whether these processes are regulated independently of one another by cellular biochemical composition. Here we demonstrate that distinct modes of mitochondrial metabolism support differentiation and effector functions of mouse T helper 1 (T_H1) cells by biochemically uncoupling these two processes. We find that the tricarboxylic acid cycle is required for the terminal effector function of T_H1 cells through succinate dehydrogenase (complex II), but that the activity of succinate dehydrogenase suppresses T_H1 cell proliferation and histone acetylation. By contrast, we show that complex I of the electron transport chain, the malate–aspartate shuttle and mitochondrial citrate export are required to maintain synthesis of aspartate, which is necessary for the proliferation of T helper cells. Furthermore, we find that mitochondrial citrate export and the malate–aspartate shuttle promote histone acetylation, and specifically regulate the expression of genes involved in T cell activation. Combining genetic, pharmacological and metabolomics approaches, we demonstrate that the differentiation and terminal effector functions of T helper cells are biochemically uncoupled. These findings support a model in which the malate–aspartate shuttle, mitochondrial citrate export and complex I supply the substrates needed for proliferation and epigenetic remodelling early during T cell activation, whereas complex II consumes the substrates of these pathways, which antagonizes differentiation and enforces terminal effector function. Our data suggest that transcriptional programming acts together with a parallel biochemical network to enforce cell state.

T cells require mitochondrial metabolism as they exit from the naive cell state to become activated, and as they return to being resting memory cells; however, the role of mitochondrial metabolism in the differentiation and function of effector T cells is less well-understood[3–5]. Metabolite tracing studies have revealed that, whereas activated T cells use glutamine for the anaplerosis of α-ketoglutarate, activated cells decrease the rate of pyruvate entry into the mitochondria in favour of lactate fermentation[5,6]. Despite the decreased utilization of glucose-derived carbon for mitochondrial metabolism, the tricarboxylic acid (TCA) cycle has previously been shown to contribute to IFNγ production by increasing cytosolic acetyl-CoA pools via mitochondrial citrate export[7]. Additionally, the TCA cycle can contribute to the electron transport chain (ETC) by generating NADH and succinate to fuel complex I and complex II, respectively. However, the role of the ETC in the later stages of T cell activation is poorly characterized. To test the contribution of the TCA cycle to the function of effector T cells, we treated cells cultured in T_H1 conditions with the TCA-cycle inhibitor sodium fluoroacetate[8]. We titrated sodium fluoroacetate or the glycolysis inhibitor 2-deoxy-D-glucose (2DG; an inhibitor of T_H1 cell activation, used as a positive control) at day 1 of T cell culture, and assayed cell proliferation at day 3 or the expression of the *Ifng*-Katushka reporter at day 5. Although 2DG was a more-potent inhibitor than sodium fluoroacetate at lower doses, both inhibitors impaired *Ifng* transcription (Fig. 1a) and T cell proliferation (Fig. 1b) in a dose-dependent manner, which suggests that the activity of TCA-cycle enzymes is required for optimal T_H1 cell activation.

To evaluate which processes downstream of the TCA cycle contribute to the role of the TCA cycle in T-helper-cell proliferation and function, we treated T_H1 cells with inhibitors of the ETC overnight on day 2 (to evaluate proliferation) or overnight on day 4 (to evaluate cytokine production), and analysed cells the following day. Unlike impairing glycolysis with 2DG or the TCA cycle with sodium fluoroacetate, which resulted in a block of both proliferation and function, we observed a dichotomy in the role of the ETC in supporting each of these processes. Although the inhibition of complex II did not impair proliferation, blocking complex I and complex III resulted in a decrease in the number of divided cells; treatment with oligomycin displayed a modest but significant effect (Fig. 1c). Importantly, viability was not affected upon acute inhibition of ETC complexes (Extended Data Fig. 1a). Consistent with this observation, treatment with rotenone or antimycin A on day 2 resulted in cell-cycle arrest at the G2 or M phase, whereas treatment with dimethyl malonate (DMM) or oligomycin did not alter cell-cycle status (Extended Data Fig. 1b). Similar to cells cultured in T_H1 conditions, cells cultured in T_H2 or T_H17 conditions displayed defects in proliferation and an altered cell cycle when treated with rotenone (Extended Data Fig. 2a, b, e, f), which suggests that complex I supports cell division regardless of the cytokine environment.

Further illustrating distinct roles for complex I and complex II in T-helper-cell proliferation and function, we observed that the ATP citrate lysase (ACLY) inhibitor BMS-303141 significantly decreased IFNγ production, consistent with previous work[7], whereas the effect of inhibition of complex I or ATP synthase with rotenone or oligomycin, respectively, was not significant. By contrast, impairing complex II activity with DMM, or complex III activity with antimycin A, significantly reduced IFNγ production to levels below those observed with BMS-303141 (Fig. 1d). Together, these observations suggest that the

[1]Department of Immunobiology, Yale School of Medicine, New Haven, CT, USA. [2]Department of Pathology, Children's Hospital of Philadelphia, Philadelphia, PA, USA. [3]Department of Pathology, Yale School of Medicine, New Haven, CT, USA. [4]Program of Computational Biology and Bioinformatics, Yale University, New Haven, CT, USA. [5]Lewis-Sigler Institute for Integrative Genomics, Princeton University, Princeton, NJ, USA. [6]Department of Chemistry, Princeton University, Princeton, NJ, USA. [7]Diabetes Research Center, University of Pennsylvania, Philadelphia, PA, USA. [8]Department of Biochemistry and Molecular Biology, Mayo Clinic College of Medicine and Science, Rochester, MN, USA. [9]Applied Mathematics Program, Yale University, New Haven, CT, USA. [10]Department of Internal Medicine (Rheumatology), Yale School of Medicine, New Haven, CT, USA. [11]Howard Hughes Medical Institute, Chevy Chase, MD, USA. [12]These authors contributed equally: Will Bailis, Justin A. Shyer. *e-mail: joseph.craft@yale.edu; richard.flavell@yale.edu

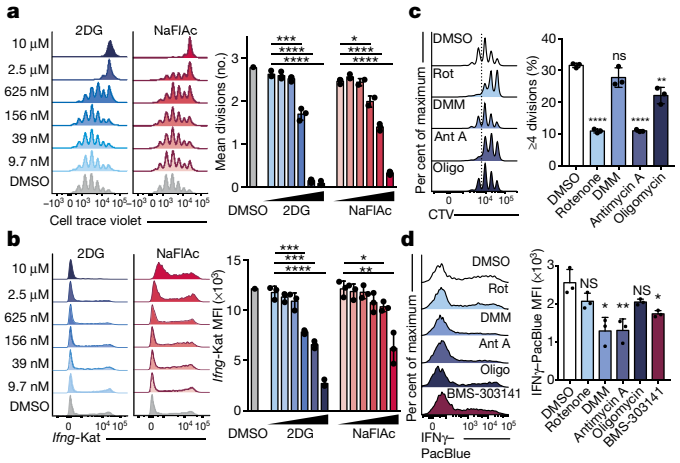

Fig. 1 | The TCA cycle supports proliferation and function of T helper cells through distinct mechanisms. a, **b**, Mean divisions at day 3 (**a**) and *Ifng*-Katushka (*Ifng*-Kat) reporter expression after restimulation with phorbol myristate acetate (PMA) and ionomycin at day 5 (**b**) of CD4 T cells cultured in T_H1 conditions with serially diluted 2DG ($n = 3$) or sodium fluoroacetate (NaFlAc) ($n = 2$ or 3). MFI, mean fluorescence intensity. **c**, **d**, Proliferation after overnight treatment on day 2 (**c**) and intracellular IFNγ protein expression after overnight treatment on day 4 (**d**) of wild-type CD4 T cells cultured in T_H1 conditions with dimethylsulfoxide (DMSO), rotenone (rot), DMM, antimycin A (ant A), oligomycin (oligo) or BMS-303141 ($n = 3$). *n*, number of technical replicates. Representative plots and a graph summarizing the results of at least two independent experiments are shown. Mean and s.d. of replicates are presented on summarized plots and unpaired, two-tailed *t*-test used to determine significance. $*P < 0.05$, $**P < 0.01$, $***P < 0.001$, $****P < 0.0001$. ns, not significant.

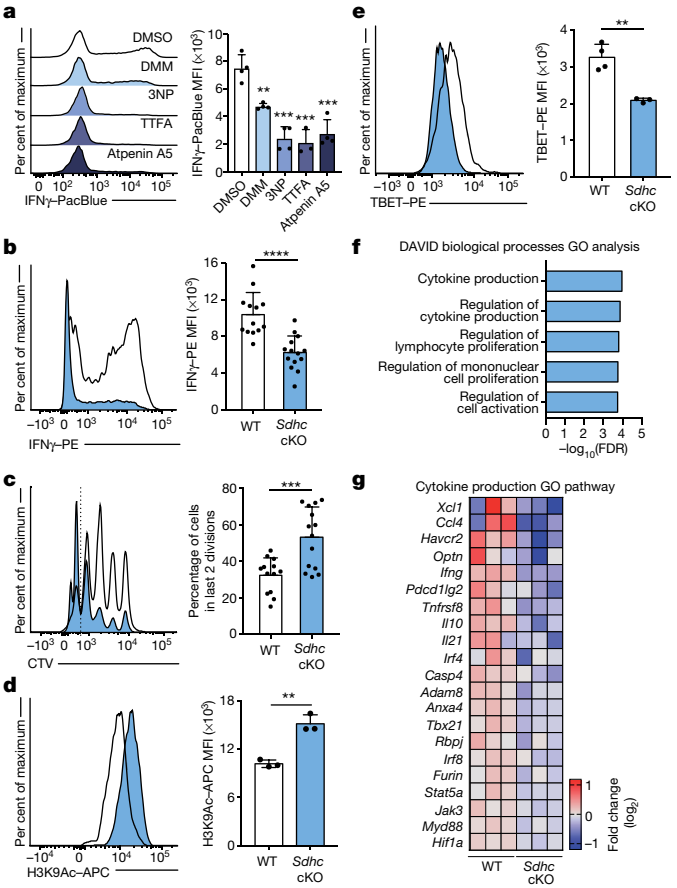

Fig. 2 | Complex II uncouples differentiation and effector function of T_H1 cells. a, Intracellular IFNγ protein expression in PMA and ionomycin-restimulated wild-type CD4 T cells cultured in T_H1 conditions at day 5 after overnight treatment with DMSO, DMM (10 mM), 3NP (1 mM), TTFA (100 μM) or atpenin A5 (1 μM) ($n = 3$). **b**, **c**, Intracellular IFNγ protein expression (**b**) and proliferation of CD4 T cells (**c**) from doxycycline-treated *Sdhc* cKO or wild-type (WT) mice cultured in T_H1 conditions at day 5. Data combined from 5 independent experiments: wild type, $n = 13$; *Sdhc* cKO, $n = 14$ biological replicates. Two-tailed *t*-test. **d**, Total cellular H3K9 acetylation (H3K9Ac) of wild-type and *Sdhc* cKO cells cultured in T_H1 conditions at day 3 ($n = 3$). Two-sided *t*-test. **e**, TBET protein expression of wild-type ($n = 4$) and *Sdhc* cKO ($n = 3$) cells cultured in T_H1 conditions at day 5. Two-sided *t*-test. **f**, DAVID Gene Ontology (GO) pathway analysis of genes that are downregulated in cKO mice compared to wild-type controls. $P < 0.05$. **g**, Heat map of gene expression from RNA-seq results for the cytokine production GO pathway. *n*, number of technical replicates, except where noted otherwise. Representative plots and a graph summarizing the results of at least two independent experiments are shown, except where noted otherwise. Mean and s.d. of replicates are presented on summarized plots and unpaired, two-tailed *t*-test used to determine significance. $**P < 0.01$, $***P < 0.001$, $****P < 0.0001$.

TCA cycle supports T_H1 function by enabling cytosolic acetyl-CoA production and by fuelling a succinate-dehydrogenase (SDH)-driven ETC. This role for the ETC was specific to the T-helper-cell cytokine culture conditions to which the cells were exposed during activation. Unlike T_H1 cells, inhibiting the ETC had a minimal effect on function of T_H2 effector cells; inhibition of complex I or complex III resulted in a slight, but significant, increase in IL-4 reporter activity (Extended Data Fig. 2c). By contrast, T_H17 cells displayed sensitivity to inhibition of both complex I and complex II (Extended Data Fig. 2d). These data indicate that the ETC has program-specific roles in regulating the effector functions of T helper cells.

To corroborate the effects of DMM on the function of T_H1 cells, we tested the capacity of three additional inhibitors of complex II—thenoyltrifluoroacetone (TTFA), 3-nitropropionic acid (3NP) and atpenin A5—to inhibit IFNγ production in T_H1 cells. Each drug impaired complex II activity, as assayed by cellular succinate accumulation (Extended Data Fig. 3a). Consistent with our results for DMM treatment, T_H1 cells treated with 3NP, TTFA or atpenin A5 produced significantly less IFNγ than control cells (Fig. 2a). In keeping with a role for the TCA cycle and complex II in promoting T_H1 cell function, cells cultured overnight with a membrane-permeable form of succinate (diethyl succinate) produced more IFNγ (Extended Data Fig. 3b). To genetically test the requirement of complex II activity in T_H1 cells, we generated a retroviral single-guide (sg)RNA expression vector (which we named MG-Guide) that is compatible with transduction of mouse T cells (Extended Data Fig. 4a, b). To validate the system, we transduced CD4 T cells with sgRNA and observed a rapid loss of protein expression when using sgRNAs that targeted *Tbx21* or *Il12rb1*, genes that are essential for T_H1-cell cytokine production; this loss led to a decrease in capacity for IFNγ production (Extended Data Fig. 4c–f, Supplementary Table 1). Transduction of T_H1 cells with a sgRNA targeting *Sdha*, which encodes the catalytic subunit of complex II, impaired capacity for IFNγ production (Extended Data Fig. 3c). To provide further genetic evidence that complex II activity is required for the function of T_H1 cells, we tested the requirement for *Sdhc*, which encodes an essential subunit of complex II. We cultured CD4 T cells isolated from $Sdhc^{fl/fl}$ *TetO-cre*$^{-/+}$ $Rosa26^{rtTA/+}$ (hereafter, *Sdhc* conditional knockout (cKO)) or $Sdhc^{+/+}$ *TetO-cre*$^{-/+}$ $Rosa26^{rtTA/+}$ control (hereafter, wild-type) mice that had been treated in vivo with doxycycline for ten days in T_H1 conditions. Unbiased mass-spectrometry analysis of metabolites in wild-type and *Sdhc* cKO T_H1 cells revealed that *Sdhc* cKO cells had increased levels of cellular succinate and α-ketoglutarate, which confirms the loss of SDH activity (Extended Data Fig. 3d, e). Consistent with our drug and sgRNA studies, *Sdhc* cKO cells produced significantly less IFNγ at day 5 post-activation (Fig. 2b). However, *Sdhc* cKO T_H1 cells proliferated significantly more than wild-type controls, which suggests that proliferation and effector function

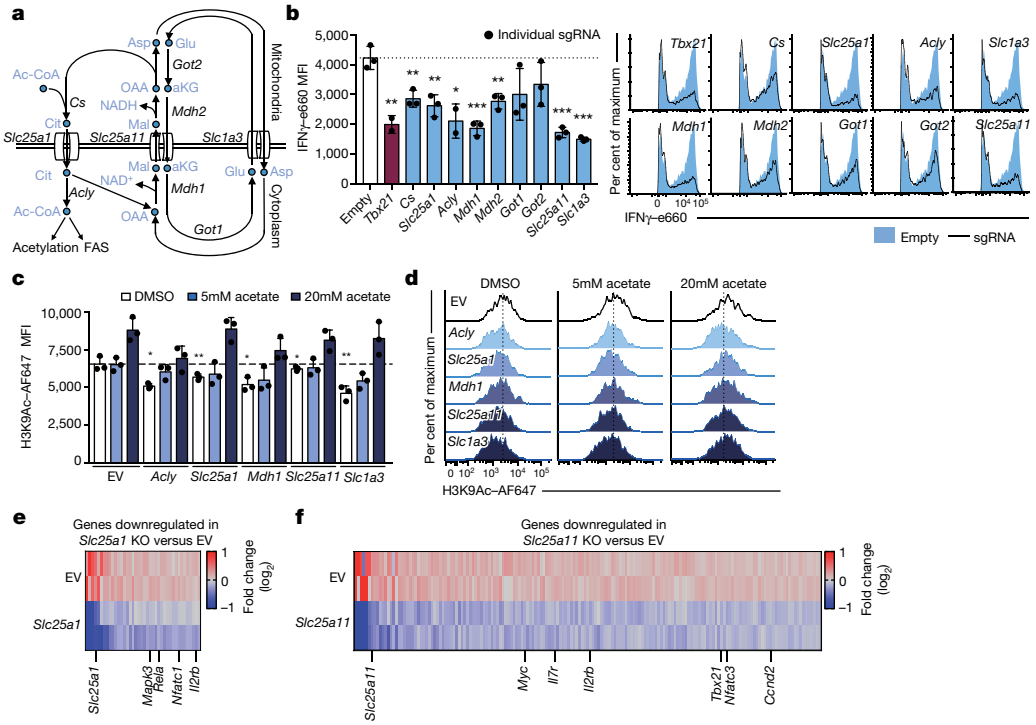

Fig. 3 | The malate–aspartate shuttle and mitochondrial citrate export are required for histone acetylation and proliferation in differentiating T_H1 cells. a, Schematic of the malate–aspartate shuttle and mitochondrial citrate export. aKG, α-ketoglutarate; Asp, aspartate; Cit, citrate; Glu, glutamate; Mal, malate; OAA, oxaloacetate. **b**, Intracellular IFNγ protein expression in Cas9-expressing CD4 T cells, transduced with sgRNAs targeting the indicated enzymes and transporters, cultured in T_H1 conditions after restimulation at day 5. Graphs show individual sgRNAs for each gene as well as the average for all three sgRNAs ($n = 2$ or 3 biological replicates). **c**, **d**, Total cellular H3K9 acetylation at day 4 of Cas9-expressing CD4 T cells transduced with sgRNAs against the indicated enzymes and transporters, in the absence or presence of 5 nM or 20 nM exogenous acetate added 1 day after transduction, cultured in T_H1 conditions ($n = 3$ technical replicates). **e**, **f**, Heat map summarizing downregulated genes determined by RNA-seq for cells expressing *Slc25a1*-targeting sgRNA (**e**) or *Slc25a11*-targeting sgRNA (**f**). $P < 0.05$. EV, empty vector; KO, knockout. Representative plots and a graph summarizing the results of at least two independent experiments are shown. Mean and s.d. of replicates are presented on summarized plots and unpaired, two-sided *t*-test used to determine significance. $^*P < 0.05$, $^{**}P < 0.01$, $^{***}P < 0.001$.

are processes that are uncoupled by complex II activity (Fig. 2c). To test whether processes in addition to proliferation that are involved in T-helper-cell differentiation were affected, we assayed the effect of SDH deficiency on histone acetylation. We found that *Sdhc* cKO cells exhibited increased H3K9 acetylation, and that DMM treatment as well as delivery of *Sdha*-targeting sgRNA increased H3K9 and H3K27 acetylation; this suggests that complex II antagonizes T-helper-cell differentiation by negatively regulating both proliferation and histone acetylation (Fig. 2d, Extended Data Fig. 5a–c).

To test the role of complex II in promoting other aspects of the functional program of T_H1 cells, we evaluated TBET protein expression in *Sdhc* cKO and wild-type cells on day 5 after activation. Consistent with defects in IFNγ production, T_H1 cells from *Sdhc* cKO mice had reduced levels of expression of TBET protein (Fig. 2e). To further investigate a role for complex II in supporting the functional program of T_H1 cells, we performed RNA sequencing (RNA-seq) on effector T_H1 cells from *Sdhc* cKO and wild-type mice at day 5 after activation. Consistent with a decrease in TBET expression, T_H1 cells from mice deficient in complex II exhibited significantly decreased expression of genes that are key to the T_H1 cell program and genes that are important during T-helper-cell activation. Notably, DAVID (Database for Annotation, Visualization and Integrated Discovery) Gene Ontology pathway analysis indicated 'cytokine production' and 'regulation of lymphocyte proliferation' as the most-dysregulated pathways (Fig. 2f, g, Extended Data Fig. 5d, e, Supplementary Table 2). These data indicate that SDH activity is a primary mechanism through which mitochondrial metabolism supports the functional programming of T_H1 cells.

We next sought to investigate which aspects of mitochondrial metabolism are antagonized by SDH to constrain proliferation. The consumption of α-ketoglutarate is known to modulate the activity of mitochondrial shuttling systems that are required to maintain the cellular redox balance and the production of key cytosolic metabolites[9–11]. The malate–aspartate shuttle and mitochondrial citrate export are two such systems; they regulate the oxidation state of nicotinamide adenine dinucleotides (NAD) in the mitochondria and the transport of acetyl-CoA from the mitochondria to the cytosol, respectively. On the basis of our data that *Sdhc* cKO T_H1 cells exhibit increased proliferation (Fig. 2c) and increased cellular α-ketoglutarate levels (Extended Data Fig. 3e), we hypothesized that these mitochondrial transport systems promote the early stages of T_H1 cell proliferation.

To test the requirement of these transport systems for T_H1 cell activation, we designed three sgRNAs per gene of interest and conducted individual sgRNA knockout experiments using MG-Guide, measuring IFNγ protein (Fig. 3a). We found that, compared to cells transduced with an empty MG-Guide vector, cells that express sgRNAs that target *Mdh1*, *Mdh2*, *Slc25a11* or *Slc1a3* produced less IFNγ protein—comparable to the levels observed with sgRNAs that target the positive-control *Tbx21* gene—as did two of the three sgRNAs designed to target *Got1* and *Got2*, which suggests that the malate–aspartate shuttle is critical during T_H1 cell activation (Fig. 3b). In addition, we observed defective IFNγ production in T_H1 cells that express sgRNA against *Cs*, *Slc25a1* and *Acly*, which indicates that citrate synthesis and export for cytosolic acetyl-CoA production are also required (Fig. 3b).

Previous reports have suggested that ACLY activity is required for T_H1-cell histone acetylation, and the ETC has previously been shown to support epigenetic remodelling[7,12]. To test the role of both shuttle systems during T_H1-cell epigenetic remodelling, we evaluated total cellular H3K9 and H3K27 acetylation. We found that impairing *Acly*, *Slc25a1*, *Mdh1*, *Slc25a11* and *Slc1a3* results in decreased H3K9 acetylation, and that acetate supplementation could compensate for these

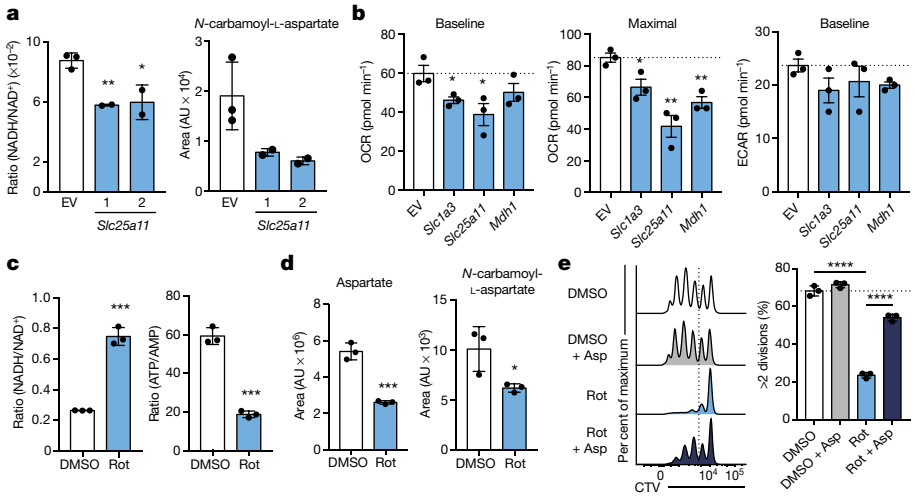

Fig. 4 | The malate–aspartate shuttle promotes complex I activity, which is required for aspartate synthesis and T-helper-cell proliferation. **a**, Cellular NADH/NAD$^+$ ratio and *N*-carbamoyl-L-aspartate measured by liquid chromatography–mass spectrometry analysis in Cas9-expressing CD4 T cells transduced with sgRNA targeting *Scl25a11*, and cultured in T_H1 conditions as described in Methods ($n = 2$ biological replicates, $n = 2$ technical replicates). AU, arbitrary units. **b**, Baseline oxygen consumption rate (OCR), maximal OCR and baseline extracellular acidification rate (ECAR) of Cas9-expressing CD4 T cells transduced with sgRNAs targeting the indicated enzymes and transporters, cultured in T_H1 conditions at day 4 ($n = 3$ biological replicates). **c**, **d**, Cellular NADH/NAD$^+$ and ATP/AMP ratios (**c**) and aspartate and *N*-carbamoyl-L-aspartate (**d**) measured by liquid chromatography–mass spectrometry analysis in wild-type CD4 T cells cultured in T_H1 conditions, and treated with DMSO or rotenone for 4 h on day 4 ($n = 3$ technical replicates). **e**, Proliferation measured at day 3 of wild-type CD4 T cells cultured in T_H1 conditions and treated on day 2 with DMSO (clear and grey bar) or rotenone (blue bars) ± 20 mM aspartate ($n = 3$ technical replicates). Representative plots and a graph summarizing the results of at least two independent experiments are shown. Mean and s.d. are presented on summarized plots and unpaired, two-sided *t*-test used to determine significance. $^*P < 0.05$, $^{**}P < 0.01$, $^{***}P < 0.001$, $^{****}P < 0.0001$.

defects (Fig. 3c, d). By contrast, H3K27 acetylation was largely unaffected by targeting these genes (with the exception of *Slc25a1*); however, the addition of acetate resulted in increased H3K27 acetylation regardless of the condition (Extended Data Fig. 6a). This effect of acetate on histone acetylation is largely explained by an increase in total H3 content, whereas the effect of the sgRNA on acetylation is only partially explained by changes in total histone mass (Extended Data Fig. 6b–d).

To evaluate the transcriptional effects of deficiency in the malate–aspartate shuttle, we performed RNA-seq at day 5 after activation on T_H1 cells that express sgRNA against *Slc25a1* or *Slc25a11*. Consistent with a role for the shuttles in promoting T_H1 cell differentiation, we observed decreased expression of genes with known roles in T cell activation and T_H1 cell programming. Targeting either of the transporters led to impaired expression of *Il2rb*, whereas loss of *Slc25a1* affected key T-cell-activation genes (such as *Nfatc1*, *Rela* and *Mapk3*) and disruption of *Slc25a11* resulted in the loss in expression of genes including *Tbx21*, *Nfatc3*, *Ccnd2* and *Myc* (Fig. 3e, f, Extended Data Fig. 6e, f, Supplementary Tables 3, 4).

Given the importance of *Il2rb, Myc* and *Ccnd2* in T-helper-cell division, we next evaluated the role of the shuttles in regulating T-helper-cell proliferation. To test this, we evaluated cell division in cells cultured in T_H1 conditions that express sgRNAs targeting *Acly*, *Slc25a1*, *Mdh1*, *Slc25a11* or *Slc1a3*. Relative to controls, targeting any of these genes resulted in modestly—but significantly—decreased proliferation (Extended Data Fig. 7). Collectively, these data demonstrate that the malate–aspartate shuttle and mitochondrial citrate export are required for T_H1 cell proliferation and transcriptional remodelling.

To investigate the biochemical mechanism that might explain these observations, we performed mass-spectrometry analysis of T cells transduced with guides targeting either *Slc25a1* or *Slc25a11* sgRNA. As expected, we found that disrupting citrate transport results in decreased levels of cellular acetyl-CoA (Extended Data Fig. 8a–c). Unexpectedly, targeting *Slc25a11* resulted in a decreased cellular NADH/NAD$^+$ ratio, which suggests that the activity of complex I is a primary mechanism by which cellular NADH/NAD$^+$ is regulated in activated T_H1 cells (Fig. 4a, Extended Data Fig. 8d, e). Moreover, targeting either shuttle system resulted in diminished levels of intermediates of the pentose phosphate pathway and of *N*-carbamoyl-L-aspartate, an essential precursor molecule for nucleotide synthesis (Fig. 4a, Extended Data Figs. 8b, c, 9a, b). Consistent with a role for the shuttling systems in providing mitochondrial NADH for the ETC, Seahorse analysis demonstrated that rates of basal and maximal oxygen consumption were impaired upon expression of sgRNAs targeting either *Mdh1*, *Slc25a11* or *Slc1a3* (Fig. 4b). This was not substantially compensated for by increased glycolysis, as the extracellular acidification rate was minimally affected (Fig. 4b).

Having observed that complex I supports early T-helper-cell proliferation and that the malate–aspartate shuttle fuels complex I (Fig. 1c), we next sought to examine the biochemical mechanism by which complex I promotes proliferation by performing mass-spectrometric analysis on rotenone-treated cells. As expected, inhibiting complex I increased the NADH/NAD$^+$ ratio and decreased the ATP/AMP ratio (Fig. 4c, Extended Data Fig. 9a, b). Rotenone treatment also led to decreased pools of cellular aspartate and *N*-carbamoyl-L-aspartate in these cells, similar to previous observations in cancer-cell lines[13,14] (Fig. 4d). To test whether this aspartate synthesis deficiency contributed to the proliferative defects of rotenone-treated cells, we supplemented rotenone-treated cells with aspartate and evaluated cell division and the cell cycle. Aspartate supplementation resulted in a significant recovery of cell proliferation, and a partial release from the arrest at the G2 or M phase following rotenone treatment (Fig. 4e, Extended Data Fig. 9c). These data demonstrate that the regulation of complex I by mitochondrial shuttling systems determines the cellular redox balance and the cytosolic aspartate availability that is required for T cell proliferation.

Using approaches that combine network-level genetic interrogation of metabolic pathways, pharmacology, transcriptomics and metabolomics, we demonstrate how T_H1 cells meet the distinct metabolic demands of differentiation and function during the course of activation. To generate the substrates needed for proliferation and epigenetic remodelling, early activated T helper cells fuel complex I through the malate–aspartate shuttle and mitochondrial citrate export. Unlike the carbon-neutral malate–aspartate shuttle (which exchanges malate for α-ketoglutarate), complex II moves carbon forward in the TCA cycle; this restricts processes that support differentiation and promotes the late-stage effector function of T_H1 cells, which permits cells to exit the

cell cycle and adopt their terminal program (Extended Data Fig. 10). These findings illustrate how differentiation and terminal effector function—previously understood to be concordantly regulated by signal transduction—are controlled by distinct metabolic modules, which elucidates how cell programming is governed by parallel transcriptional and biochemical networks.

Online content

Any methods, additional references, Nature Research reporting summaries, source data, extended data, supplementary information, acknowledgements, peer review information; details of author contributions and competing interests; and statements of data and code availability are available at https://doi.org/10.1038/s41586-019-1311-3.

Received: 8 November 2017; Accepted: 22 May 2019;
Published online 19 June 2019.

1. Buck, M. D., Sowell, R. T., Kaech, S. M. & Pearce, E. L. Metabolic instruction of immunity. *Cell* **169**, 570–586 (2017).
2. Buck, M. D., O'Sullivan, D. & Pearce, E. L. T cell metabolism drives immunity. *J. Exp. Med.* **212**, 1345–1360 (2015).
3. Klein Geltink, R. I. et al. Mitochondrial priming by CD28. *Cell* **171**, 385–397.e11 (2017).
4. Buck, M. D. et al. Mitochondrial dynamics controls T cell fate through metabolic programming. *Cell* **166**, 63–76 (2016).
5. Chang, C.-H. et al. Posttranscriptional control of T cell effector function by aerobic glycolysis. *Cell* **153**, 1239–1251 (2013).
6. Wang, R. et al. The transcription factor Myc controls metabolic reprogramming upon T lymphocyte activation. *Immunity* **35**, 871–882 (2011).
7. Peng, M. et al. Aerobic glycolysis promotes T helper 1 cell differentiation through an epigenetic mechanism. *Science* **354**, 481–484 (2016).
8. Peters, R. *Biochemical Lesions and Lethal Synthesis* (Pergamon, 1963).
9. Contreras, L. & Satrústegui, J. Calcium signaling in brain mitochondria: interplay of malate aspartate NADH shuttle and calcium uniporter/mitochondrial dehydrogenase pathways. *J. Biol. Chem.* **284**, 7091–7099 (2009).
10. Safer, B. The metabolic significance of the malate-aspartate cycle in heart. *Circ. Res.* **37**, 527–533 (1975).
11. LaNoue, K. F. & Williamson, J. R. Interrelationships between malate-aspartate shuttle and citric acid cycle in rat heart mitochondria. *Metabolism* **20**, 119–140 (1971).
12. Wellen, K. E. et al. ATP-citrate lyase links cellular metabolism to histone acetylation. *Science* **324**, 1076–1080 (2009).
13. Birsoy, K. et al. An essential role of the mitochondrial electron transport chain in cell proliferation is to enable aspartate synthesis. *Cell* **162**, 540–551 (2015).
14. Sullivan, L. B. et al. Supporting aspartate biosynthesis is an essential function of respiration in proliferating cells. *Cell* **162**, 552–563 (2015).

METHODS

T cell assays and sgRNA delivery. CD4 T cells were isolated from constitutive Cas9-expressing (Cas9tg) B6 mice[15], stimulated with anti-CD3 and anti-CD28 coated beads (Miltenyi T Cell Activation/Expansion Kit, mouse), and cultured in assay-determined T_H1 conditions (5 ng/ml IL-2, 2 ng/ml IL-12 and 10 μg/ml anti-IL-4). On day 1 post-activation, T cells were transduced with MG-Guide retrovirus using spin transduction at 1,200*g* for 90 min at 37 °C. IFNγ cytokine was measured by adding brefeldin A, 1 h after the addition of PMA (20 ng/ml) and ionomycin (20 ng/ml); 4 h after restimulation, cells were fixed, stained with anti-CD4 (Biolegend), anti-GFP (Millipore) and anti-IFNγ (Biolegend), and analysed by flow cytometry. To assay for *Ifng*-Katushka, IL-4–GFP, and IL-17–GFP expression, T cells from *Ifng*-Katushka[16], 4GET (Jackson Labs, 004190) and IL-17–GFP (Jackson Labs, 018472) reporter mice were activated with PMA and ionomycin for four hours, stained with anti-CD4 and then analysed by flow cytometry for reporter activity in GFP^+ cells. Cell division was measured by labelling cells with CellTrace Violet (Thermo) before activation, and evaluated for proliferation at day 3 after activation; where indicated, inhibitors and metabolites were added to the medium overnight on day 2 after activation. Cell-cycle status was determined by intracellular flow cytometry analysis of Ki67 and DAPI, at day 3 after activation; where indicated, inhibitors and metabolites were added to the medium overnight on day 2 after activation. Mitochondrial reactive oxygen species was measured by flow cytometry in CD4 T cells by staining cells with MitoSOX Red mitochondrial superoxide indicator (Thermo) and anti-CD4 for 30 min at 37 °C in the presence of the indicated inhibitors. For all experiments using inhibitors or metabolite supplementation, the following doses were used: 1 μM rotenone (Sigma), 10 mM DMM (Sigma), 1 mM 3NP (Sigma), 100 μM TTFA (Sigma), 1 μM atpenin A5 (Cayman Chemical), 1 μM antimycin A (Sigma), 1 μM oligomycin (Sigma), 5mM diethyl succinate (Sigma) or 20mM aspartate. All mice required for this study were housed and maintained under specific-pathogen-free conditions in the animal facility of the Yale University School of Medicine, and all corresponding animal protocols were approved by the Institutional Animal Care and Use Committee (IACUC) of Yale University. This study was conducted in compliance with all relevant ethical regulations. All cells used for experimentation were collected from male and female mice at 6–8 weeks of age.

MG-Guide vector generation, sgRNA cloning and retroviral production. MG-Guide was generated by removing the IRES element from MIGR1 (Addgene) by EcoRI and NotI digestion, and adding the human U6 promoter and SV40 promoter from pMKO-GFP (Addgene) by infusion assembly (Clonetech). To add the sgRNA cloning site, the vector was digested with AgeI and EcoRI and combined by infusion assembly with an IDT Gene Block containing two BbsI restriction sites upstream of a scaffold RNA sequence and a U6 stop. To clone individual sgRNAs, MG-Guide was digested with BbsI and pairs of oligonucleotides (Sigma) with complimentary overhangs were annealed and ligated into the vector. For retroviral production, 1 μg of MG-Guide plasmid and 0.5 μg of EcoHelper plasmid were transfected into 5×10^5 HEK293T cells (source ATCC, identity unconfirmed, not tested for mycoplasma) in a 6-well plate using X-tremeGENE 9 DNA Transfection Reagent (Roche) overnight. The medium was then replaced, and virus was collected 24 h later. Isolated CD4 T cells (1×10^6) were stimulated overnight, and spin-transduced in the viral preparation with 1 μg/ml polybrene at 1,200*g* for 90 min at 37 °C.

RNA-seq analysis. Raw reads from RNA-seq were aligned to the mouse genome mm10 with STAR 2.7.0[17], and gene-expression levels were measured by HTSeq 0.11.1[18]. Subsequently, differential expression analysis between different groups was performed with DESeq2[19].

Seahorse analysis. Analysis was performed on cells at day 3, day 4 and day 5 after activation. Cells were washed three times in complete Seahorse medium (Seahorse Bioscience) with 10 mM glucose, 1 mM sodium pyruvate and 2 mM glutamine. Cells were plated at 4×10^4 cells per well in a 96-well Seahorse assay plate, pre-treated with poly-D-lysine. Cells were equilibrated to 37 °C for 30 min before assay. OCR (pmoles/min) and ECAR (mpH/min) were measured as indicated upon cell treatment with oligomycin (0.5 mM), FCCP (0.2 mM), rotenone (1 μM), DMM (10 mM) and antimycin A (1 μM), according to the manufacturer's instructions.

Metabolome extraction. Cells were seeded at 1×10^6 cells/ml and incubated for 4 h in complete RPMI containing dialysed FBS medium. Cells were then transferred to 1.5-ml tubes and pelleted (1 min, 6,000*g*, at room temperature). Medium was removed by aspiration and the cells were washed once with 500 μl of PBS. Metabolome extraction was performed by the addition of 50 μl of ice cold solvent (40:40:20 acetonitrile:methanol:water + 0.5% formic acid). After a 5-min incubation on ice, acid was neutralized by the addition of NH_4HCO_3. After centrifugation (15 min, 16,000*g*, at 4 °C), the clean supernatant was transferred to a clean tube, frozen on dry ice and kept at -80 °C until liquid chromatography–mass spectrometry (LC–MS) analysis[20].

Succinate quantification. Wild-type CD4 T cells (1×10^6) were activated under T_H1 culture conditions. After 4 days, cells were replated into fresh medium and cultured with DMSO, 10 mM DMM, 1 mM 3NP, 100 μM TTFA or 1 μM atpenin A5 for 6 h. Cells were then collected, processed and analysed using the Succinate Assay Kit (Abcam) according to the manufacturer's protocol.

LC–MS analysis. Cell extracts were analysed using a quadrupole–orbitrap mass spectrometer (Q Exactive, Thermo Fisher Scientific) coupled to hydrophilic interaction chromatography via electrospray ionization. Liquid chromatography separation was on a XBridge BEH Amide column (2.1 mm × 150 mm, 2.5-μm particle size; Waters) using a gradient of solvent A (20 mM ammonium acetate, 20 mM ammonium hydroxide in 95:5 water:acetonitrile, pH 9.45) and solvent B (acetonitrile). Flow rate was 150 μl/min, column temperature was 25 °C, autosampler temperature was 5 °C and injection volume was 10 μl. The liquid chromatography gradient was: 0 min, 90% B; 2 min, 85% B; 3 min, 75% B; 7 min, 75% B; 8 min, 70% B; 9 min, 70% B; 10 min, 50% B; 12 min, 50% B; 13 min, 25% B; 14 min, 25% B; 16 min, 0% B; 21 min, 0% B; 22 min, 90% B; 25 min, 90% B. Autosampler temperature was 5 °C and injection volume was 10 μl. The mass spectrometer was operated in negative-ion mode to scan from *m/z* 70 to 1,000 at 1 Hz and a resolving power of 140,000[21]. Data were analysed using the MAVEN software[22].

Statistical analysis. Experiments were conducted with technical and biological replicates at an appropriate sample size, as estimated by our prior experience. No statistical methods were used to predetermine sample size. No methods of randomization and no blinding were applied. All data were replicated independently at least once as indicated in the figure legends, and all attempts to reproduce experimental data were successful. For all bar graphs, mean + s.d. are shown. All statistical analysis was performed using GraphPad Prism 7 (or more recent versions). *P* values < 0.05 were considered significant; $*P < 0.05$, $**P < 0.01$, $***P < 0.001$, $****P < 0.0001$; *P* values > 0.05 were considered as non-significant. FlowJo 8.0 (or more recent versions) (Treestar) was used to analyse flow cytometry data. All sample sizes and statistical tests used are detailed in each figure legend.

Reporting summary. Further information on research design is available in the Nature Research Reporting Summary linked to this paper.

Data availability

The data that support the findings of this study are available from the corresponding authors upon reasonable request. RNA-seq datasets have been deposited in Gene Expression Omnibus under the accession number GSE130713.

15. Platt, R. J. et al. CRISPR-Cas9 knockin mice for genome editing and cancer modeling. *Cell* **159**, 440–455 (2014).
16. Gagliani, N. et al. Coexpression of CD49b and LAG-3 identifies human and mouse T regulatory type 1 cells. *Nat. Med.* **19**, 739–746 (2013).
17. Dobin, A. et al. STAR: ultrafast universal RNA-seq aligner. *Bioinformatics* **29**, 15–21 (2013).
18. Anders, S., Py, P. T. & Huber, W. HTSeq—a Python framework to work with high-throughput sequencing data. *Bioinformatics* **31**, 166–169 (2015).
19. Love, M. I., Huber, W. & Anders, S. Moderated estimation of fold change and dispersion for RNA-seq data with DESeq2. *Genome Biol.* **15**, 550 (2014).
20. Lu, W., Wang, L., Chen, L., Hui, S. & Rabinowitz, J. D. Extraction and quantitation of nicotinamide adenine dinucleotide redox cofactors. *Antioxid. Redox Signal.* **28**, 167–179 (2018).
21. Jang, C. et al. The small intestine converts dietary fructose into glucose and organic acids. *Cell Metab.* **27**, 351–361.e3 (2018).
22. Melamud, E., Vastag, L. & Rabinowitz, J. D. Metabolomic analysis and visualization engine for LC-MS data. *Anal. Chem.* **82**, 9818–9826 (2010).

Acknowledgements This work was supported by NIH grants R37 AR40072, R61AR073048 (J.C. and R.A.F.), F31 AI1333855 (J.A.S.), T32 AI7019-41 (J.A.S.), R01 CA166025-04 (L.J.M. III), T32 GM065841-14 (L.J.M. III), the Howard Hughes Medical Institute (R.A.F.), European Union's Horizon 2020, and Marie Sklodowska-Curie grant agreement no. 751423 (J.C.G.C.), and the Paradifference Foundation (L.J.M. III).

Author contributions W.B., J.A.S., J.C. and R.A.F. designed the study and wrote the manuscript. W.B. and J.A.S. designed and performed experiments. J.Z., R.Q. and Y.K. performed all bioinformatic and genomic analysis. P.B. assisted with sequencing. J.C.G.C. and J.R. designed and performed LC–MS experiments and data analysis. F.J.A.K. and L.J.M. III prepared and provided *Sdhc* cKO mouse tissue. O.K. assisted with vector cloning. H.R.S. assisted with experimentation. R.J. assisted with experimental design. All authors edited and approved the manuscript.

Competing interests R.A.F. is a founder, shareholder and advisor for Rheos Medicines, Inc.

Additional information

Supplementary information. is available for this paper at https://doi.org/10.1038/s41586-019-1311-3.

Correspondence and requests for materials should be addressed to J.C. or R.A.F.

Peer review information *Nature* thanks Navdeep Chandel and the other anonymous reviewer(s) for their contribution to the peer review of this work.

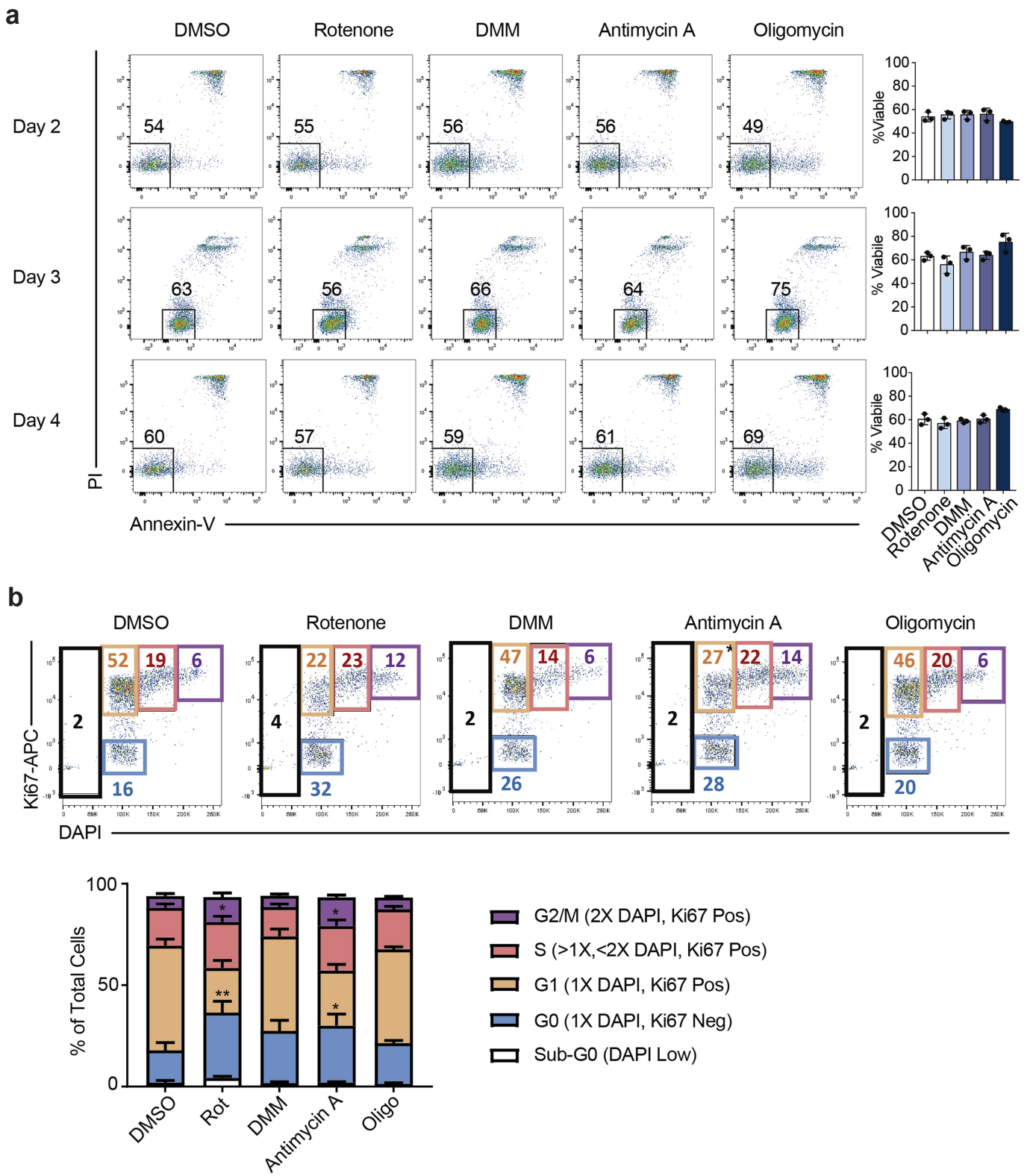

Extended Data Fig. 1 | Acute ETC inhibition alters cell cycle, but not viability, in T_H1 cells. a, Viability measured by propidium iodide (PI) and annexin-V staining of wild-type CD4 T cells cultured in T_H1 conditions and treated overnight for 16 h on day 1, 2 or 3 of culture with DMSO, rotenone, DMM, antimycin A or oligomycin ($n = 3$). **b**, Cell-cycle analysis measured by Ki67 and DAPI of CD4 T cells cultured in T_H1 conditions on day 3 following 16-h overnight treatment with DMSO ($n = 5$), rotenone, DMM, antimycin A or oligomycin ($n = 6$). *n*, number of technical replicates. Representative plots and a graph summarizing the results of three independent experiments are shown. Mean and s.d. of replicates are presented on summarized plots and unpaired, two-tailed *t*-test used to determine significance. $^*P < 0.05$, $^{**}P < 0.01$.

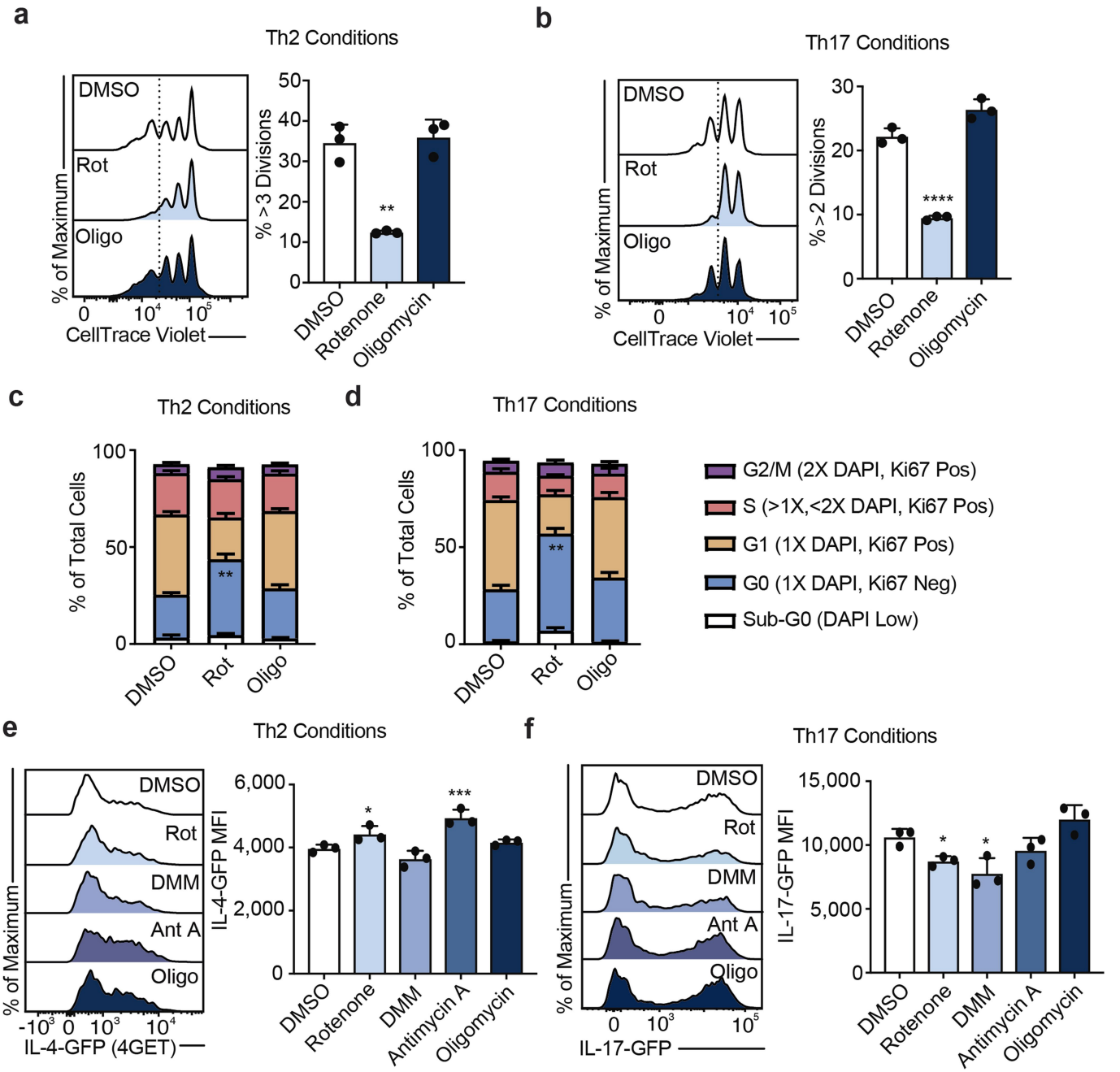

Extended Data Fig. 2 | ETC regulation of proliferation is conserved among subtypes of T helper cells, but ETC requirements for effector cytokine transcription differ between T_H1, T_H2 and T_H17 cells. **a**, **b**, Proliferation of wild-type CD4 T cells cultured in T_H2 (**a**) and T_H17 (**b**) conditions, following 16-h overnight treatment with DMSO, rotenone or oligomycin ($n = 3$). **c**, **d**, Cell-cycle analysis measured by Ki67 and DAPI of CD4 T cells cultured in T_H2 (**c**) and T_H17 (**d**) conditions on day 3 following 16-h overnight treatment with DMSO, rotenone, DMM, antimycin A or oligomycin ($n = 6$). **e**, **f**, Effector cytokine transcription after PMA and ionomycin restimulation at day 5 measured by IL-4–GFP (4GET) reporter expression in cells cultured in T_H2 conditions (**e**) and IL17–GFP reporter expression in cells cultured in T_H17 conditions (**f**) following 16-h overnight treatment with DMSO, rotenone, DMM, antimycin A or oligomycin ($n = 3$). *n*, number of technical replicates. Representative plots and a graph summarizing the results of three independent experiments are shown. Mean and s.d. of replicates are presented on summarized plots and unpaired, two-tailed *t*-test used to determine significance. $^*P < 0.05$, $^{**}P < 0.01$, $^{***}P < 0.001$, $^{****}P < 0.0001$.

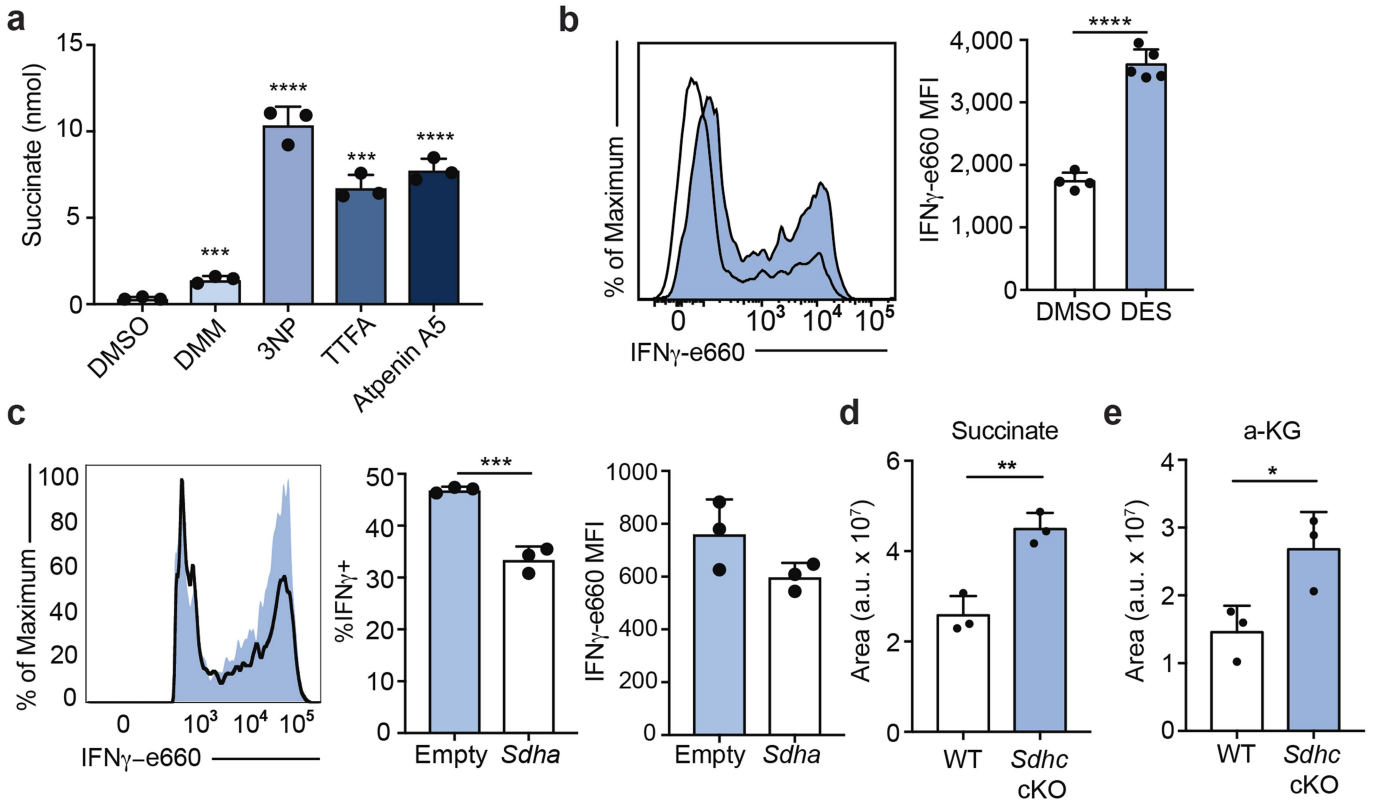

Extended Data Fig. 3 | Complex II inhibition is functional and leads to a loss of IFNγ production in T_H1 cells. a, Cellular succinate at day 5 evaluated using Succinate Assay Kit (Abcam) in wild-type CD4 T cells cultured in T_H1 conditions following 6-h treatment with DMSO, 10 mM DMM, 1 mM 3NP, 100 μM TTFA or 1 μM atpenin A5 ($n = 3$). **b**, IFNγ protein production after PMA and ionomycin restimulation at day 5 of wild-type CD4 T cells cultured in T_H1 conditions following 16-h overnight treatment with 10 mM diethyl succinate (DES) ($n = 5$) or DMSO ($n = 4$). **c**, IFNγ protein production after PMA and ionomycin restimulation at day 5 of Cas9-expressing CD4 T cells cultured in T_H1 conditions transduced with one of three individual sgRNA targeting *Sdha*, or an empty-vector control ($n = 3$ biological replicates). **d**, **e**, Total cellular succinate (**d**) and α-ketoglutarate (**e**) measured by LC–MS analysis in wild-type or *Sdhc* cKO CD4 T cells cultured in T_H1 conditions after 4-h culture in dialysed FBS-containing medium at day 5 ($n = 3$). *n*, number of technical replicates, unless otherwise stated. Representative plots and a graph summarizing the results of at least two independent experiments are shown. Mean and s.d. of replicates are presented on summarized plots and unpaired, two-tailed *t*-test used to determine significance. $^*P < 0.05$, $^{**}P < 0.01$, $^{***}P < 0.001$, $^{****}P < 0.0001$.

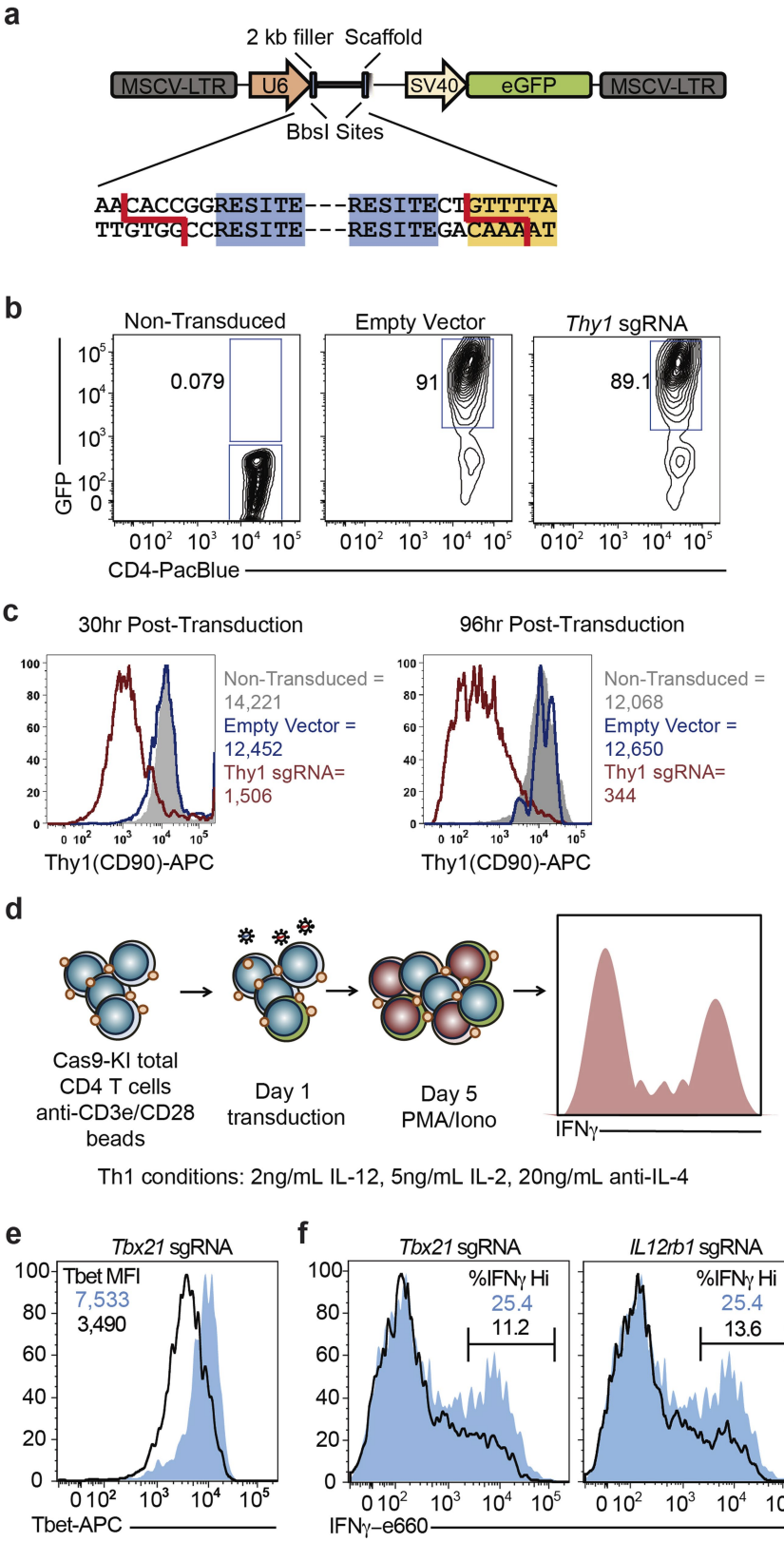

Extended Data Fig. 4 | See next page for caption.

Extended Data Fig. 4 | Retroviral expression of sgRNA in Cas9-expressing CD4 T cells. a, Schematic of MG-Guide retroviral vector. **b**, CD4 T cells from Cas9-expressing mice were stimulated with anti-CD3 and anti-CD28 coated beads for 24 h and retrovirally transduced with either a MG-Guide (empty vector) or a MG-Guide vector cloned to express a sgRNA against *Thy1* (*Thy1* sgRNA). GFP expression was measured at 24 h after transduction, compared to non-transduced cells. **c**, THY1.1 protein expression was measured in transduced (empty vector blue line; *Thy1* sgRNA red line) and non-transduced (solid grey) cells by flow cytometry at 30 and 96 h after transduction. **d**, Schematic of experimental design for functional T_H1 sgRNA studies. **e**, CD4 T cells from Cas9-expressing mice were stimulated with anti-CD3 and anti-CD28 beads in IL-2 (5 ng ml^{-1}), anti-IL-4 (10 μg ml^{-1}) and IL-12 (2 ng ml^{-1}) and retrovirally transduced 24 h after activation with either empty MG-Guide (shaded blue) or MG-Guide expressing a sgRNA against *Tbx21* (outline). TBET protein expression was measured by intracellular flow cytometry on day 3. **f**, Cas9-expressing CD4 T cells were cultured as above, and infected with MG-Guide, a sgRNA against *Tbx21* or a sgRNA against *Il12rb*. IFNγ protein was measured by intracellular flow cytometry on day 5 after restimulation with PMA (20 ng ml^{-1}) and ionomycin (1 μg ml^{-1}).

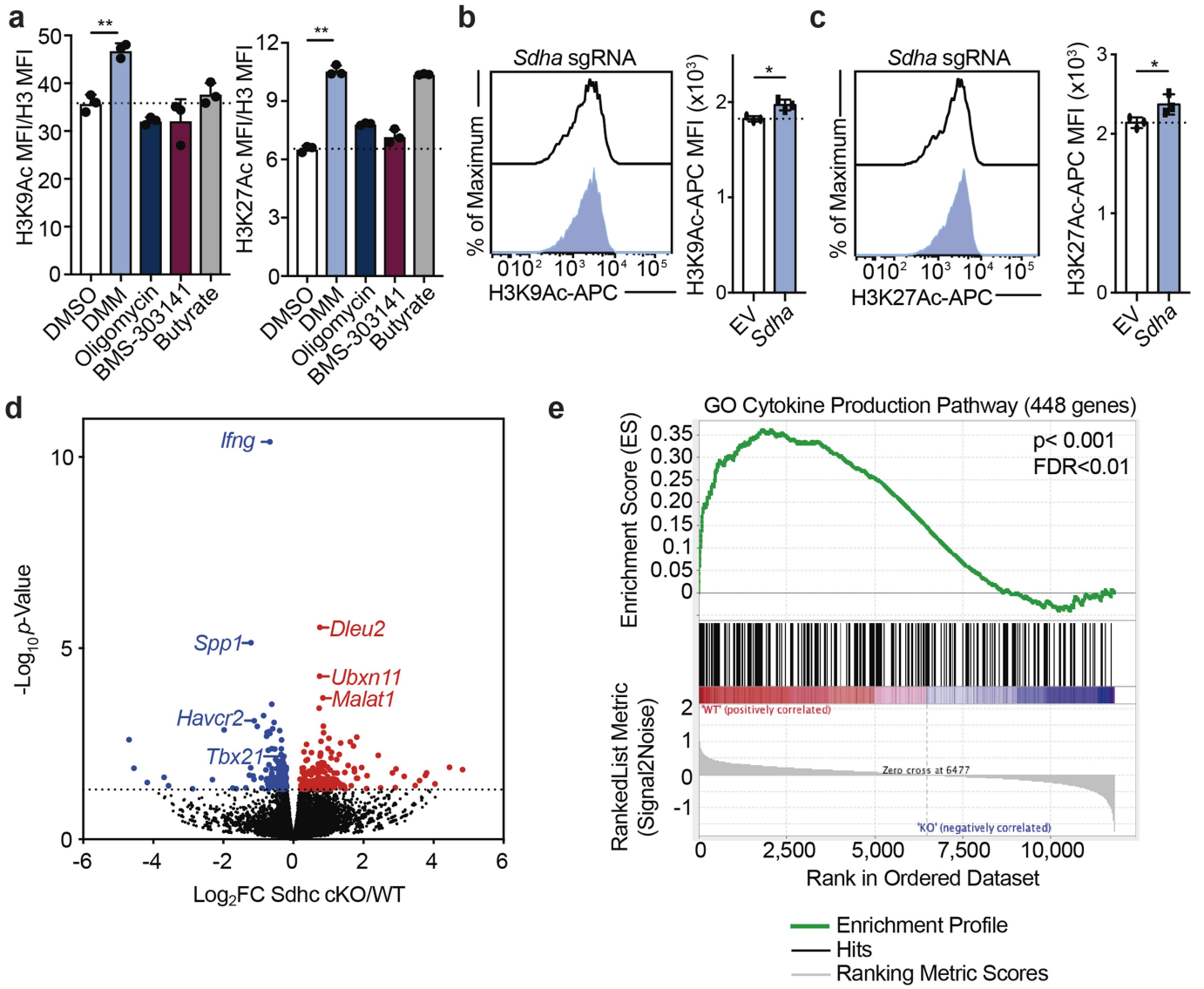

Extended Data Fig. 5 | Complex II regulates epigenetic modifications and program-specific gene expression in T_H1 cells. a, H3K9 acetylation and H3K27 acetylation, normalized to total cellular H3 and 1× DNA content on day 3 of wild-type CD4 T cells cultured in T_H1 conditions after 16-h overnight treatment with DMSO, DMM, oligomycin, BMS-303141 or butyrate ($n = 3$). **b**, **c**, H3K9 acetylation (**b**) and H3K27 acetylation (**c**) at day 5 of Cas9-expressing CD4 T cells cultured in T_H1 conditions transduced with one of three individual sgRNA targeting *Sdha*, or an empty-vector control ($n = 3$ biological replicates). **d**, **e**, Volcano plot summarizing RNA-seq data that indicate the most-differentially regulated transcripts between wild-type and *Sdhc* cKO T_H1 cells (**d**) and gene set enrichment analysis (GSEA) plot of the GO cytokine production pathway (**e**) ($n = 3$ biological replicates). *n*, number of technical replicates unless otherwise stated. Representative plots and a graph summarizing the results of at least two independent experiments are shown. Mean and s.d. of replicates are presented on summarized plots and unpaired, two-tailed *t*-test used to determine significance. $^*P < 0.05$, $^{**}P < 0.01$.

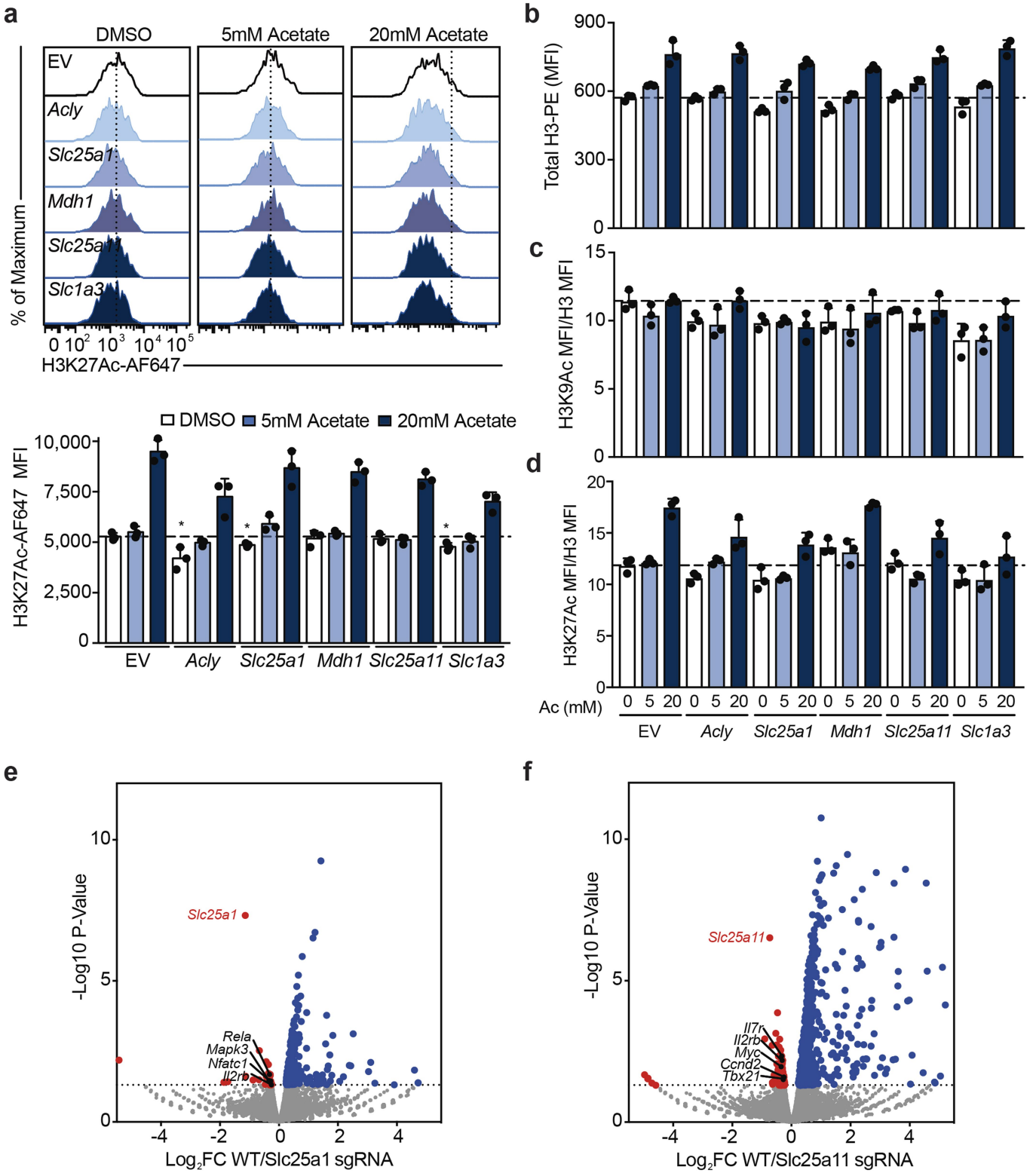

Extended Data Fig. 6 | The malate–aspartate shuttle and mitochondrial citrate export dynamically regulate histone acetylation and program-specific gene expression in T_H1 cells. a–d, H3K27 acetylation (**a**), total cellular H3 (**b**), H3K9 acetylation normalized to total cellular H3 and 1× DNA content (**c**) and H3K27 acetylation normalized to total cellular H3 and 1× DNA content (**d**) on day 4 of Cas9-expressing CD4 T cells transduced with three individual sgRNAs targeting *Acly*, *Slc25a1*, *Mdh1*, *Slc25a11* or *Slc1a3*, or empty vector, cultured in T_H1 conditions ($n = 3$ biological replicates). **e**, **f**, Volcano plot summarizing RNA-seq data that indicate the most-differentially regulated transcripts at day 5 in Cas9-expressing CD4 T cells cultured in T_H1 conditions transduced with empty vector or one sgRNA targeting *Slc25a1* (**e**) or *Slc25a11* (**f**) ($n = 2$ biological replicates). Representative plots and a graph summarizing the results of at least two independent experiments are shown. Mean and s.d. of replicates are presented on summarized plots and unpaired, two-tailed *t*-test used to determine significance. $^*P < 0.05$.

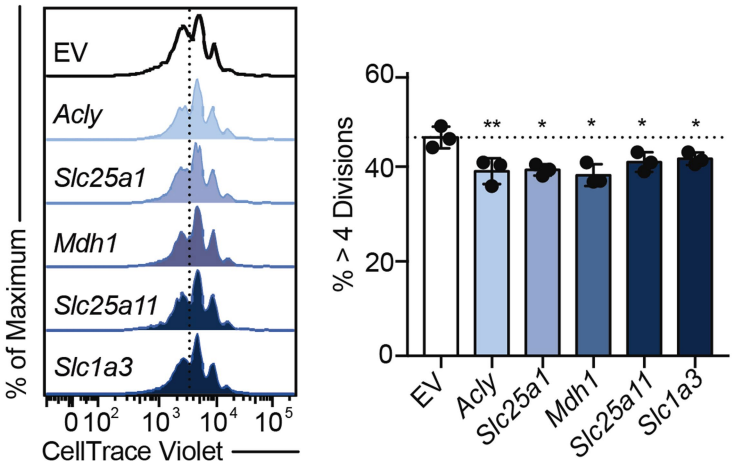

Extended Data Fig. 7 | The malate–aspartate shuttle and mitochondrial citrate export are required for proliferation in T_H1 cells. Proliferation of Cas9-expressing CD4 T cells transduced with empty-vector control or one of three individual sgRNAs targeting *Acly*, *Slc25a1*, *Mdh1*, *Slc25a11* or *Slc1a3*, cultured in T_H1 conditions at day 5 ($n = 3$ biological replicates). Representative plots and a graph summarizing the results of at least two independent experiments are shown. Mean and s.d. of replicates are presented on summarized plots and unpaired, two-tailed *t*-test used to determine significance. $^*P < 0.05$, $^{**}P < 0.01$.

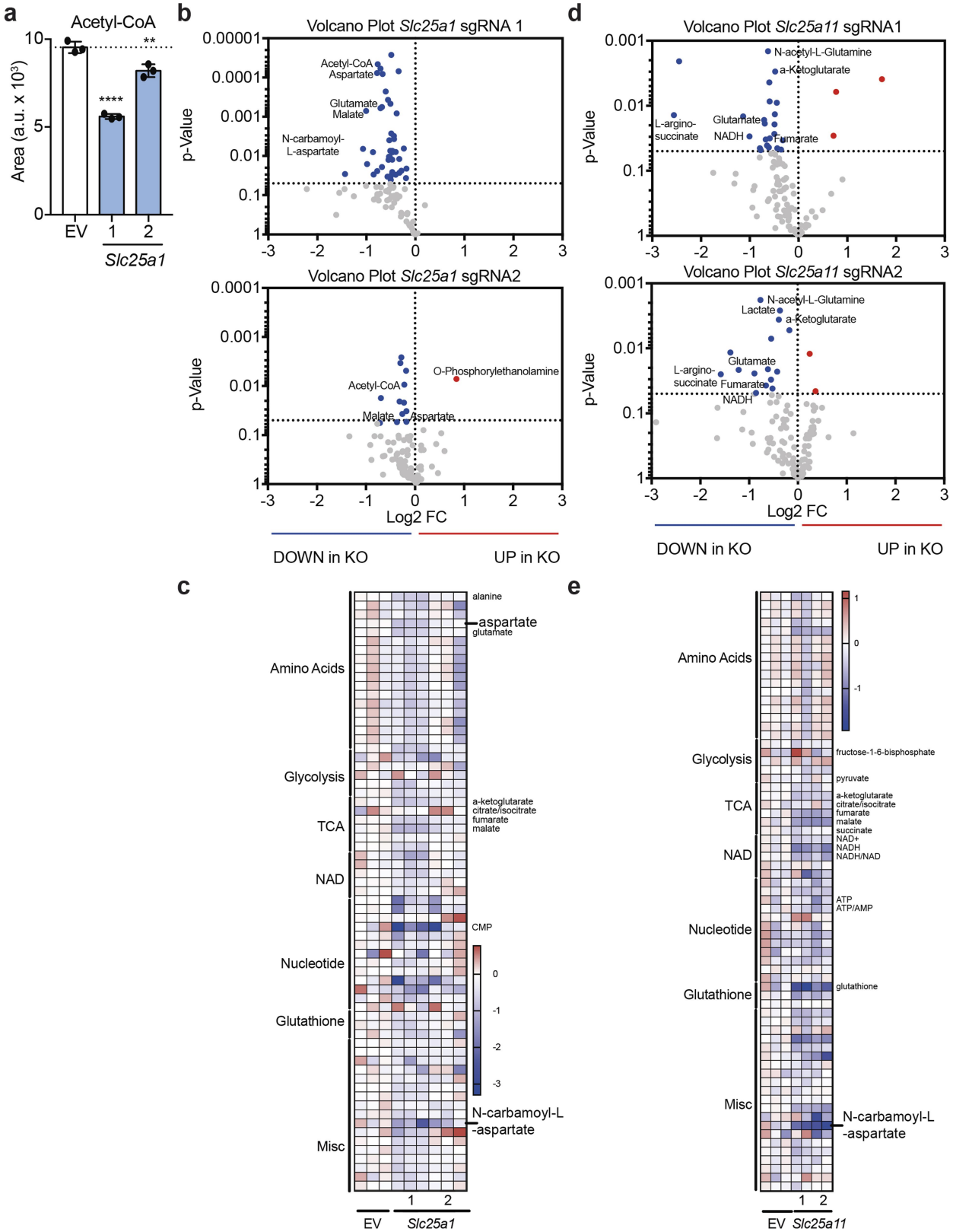

Extended Data Fig. 8 | The malate–aspartate shuttle and mitochondrial citrate export regulate levels of cellular acetyl-CoA and cellular metabolism. a, Cellular acetyl-CoA measured by LC–MS analysis in Cas9-expressing CD4 T cells transduced with empty vector or two individual sgRNAs targeting *Slc25a1*, as described, on day 5 of culture in T_H1 conditions ($n = 2$ biological replicates, $n = 3$ technical replicates). a.u., arbitrary units. **b**, **c**, Volcano plot (**b**) and heat map (**c**) of all metabolites measured by LC–MS analysis in Cas9-expressing CD4 T cells transduced with empty vector or two individual sgRNAs targeting *Slc25a1*, as described, on day 5 of culture in T_H1 conditions ($n = 2$ biological replicates, $n = 3$ technical replicates). **d**, **e**, Volcano plot (**d**) and heat map (**e**) of all metabolites measured by LC–MS analysis in Cas9-expressing CD4 T cells transduced with empty vector or two individual sgRNAs targeting *Slc25a1*, as described, on day 5 of culture in T_H1 conditions ($n = 2$ biological replicates, $n = 2$ technical replicates). Mean and s.d. of replicates are presented on summarized plots and unpaired, two-tailed *t*-test used to determine significance. $^{**}P < 0.01$, $^{****}P < 0.0001$.

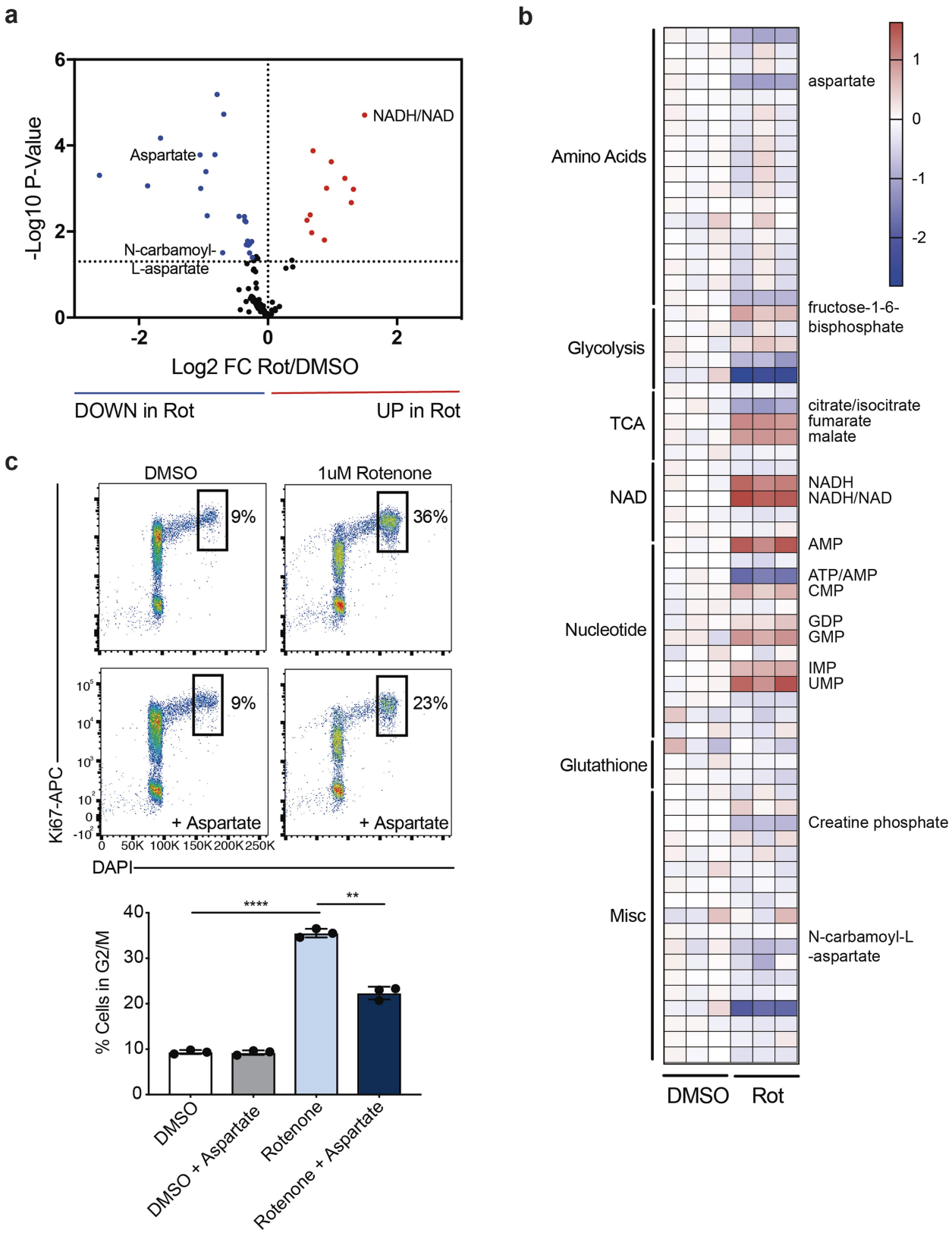

Extended Data Fig. 9 | Complex I activity is required for aspartate production and cell-cycle progression in activating T_H1 cells. **a**, **b**, Volcano plot (**a**) and heat map (**b**) of all metabolites measured by LC–MS analysis in wild-type CD4 T cells treated acutely for 4 h on day 5 of culture in T_H1 conditions ($n = 3$). **c**, Cell-cycle analysis using Ki67 and DAPI of wild-type CD4 T cells cultured in T_H1 conditions at day 3 following 16-h overnight treatment with DMSO or rotenone ± 20 mM aspartate ($n = 3$). *n*, number of technical replicates. Representative plots and a graph summarizing the results of at least two independent experiments are shown. Mean and s.d. of replicates are presented on summarized plots and unpaired, two-tailed *t*-test used to determine significance. $^{**}P < 0.01$, $^{****}P < 0.0001$.

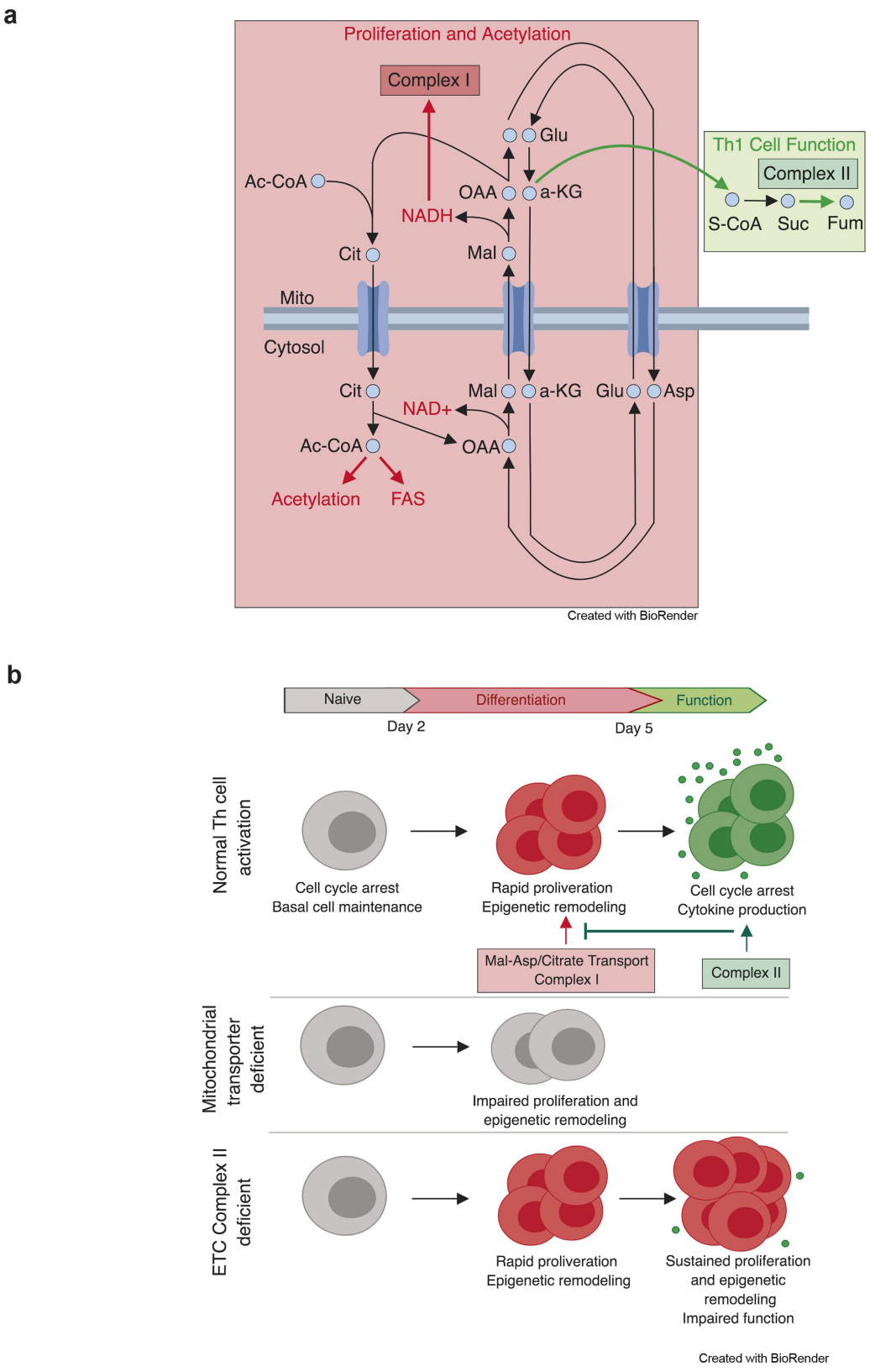

Extended Data Fig. 10 | See next page for caption.

Extended Data Fig. 10 | Conceptual models of mitochondrial metabolite transport and the consequence of metabolic perturbations on T_H1 cell activation. a, Early-stage T_H1 cell activation is supported by the malate–aspartate shuttle and mitochondrial citrate export. These mitochondrial transport systems provide the key substrates that are needed for cell division and histone acetylation. Citrate export results in the production of cytosolic acetyl-CoA that can be used to synthesize the fatty acids that are needed for plasma membrane expansion during division, as well as the acetyl groups that are used for histone acetylation. Interconnected with this export pathway is the malate–aspartate shuttle, a carbon-neutral cycle that results in the net movement of NAD^+ to the cytosol and NADH into the mitochondria, through which the cycle can fuel the activity of ETC complex I. Through the activity of complex I, NAD^+ can be continually recycled, which enables the production of aspartate (an essential precursor for nucleotide synthesis). These processes are antagonized by the activity of SDH (ETC complex II), which consumes α-ketoglutarate; this limits the availability of the latter for the malate–aspartate shuttle and promotes effector functions of T_H1 cells. **b**, T-helper-cell activation is defined by two major phases: (1) a period of rapid division and epigenetic remodelling, and (2) cell-cycle arrest and cytokine production. Each of these phases is supported by a discrete component of mitochondrial metabolism. The malate–aspartate shuttle and mitochondrial citrate export generate the material needed for early-phase cell differentiation to occur. As differentiation continues, the activity of complex II draws carbon away from the shuttle, and thus acts to pull activated T_H1 cells out of the differentiation process and to enable them to fully engage their terminal effector cell program. When the mitochondrial transport networks are disrupted, T_H1 cells are unable to properly proliferate or epigenetically reprogram. By contrast, inhibiting the activity of complex II causes activated T_H1 cells to continuously proliferate and remodel their chromatin, which prevents them from exiting the differentiation phase and engaging their terminal effector program.

nature research

Corresponding author(s): Flavell RA, Craft J

Last updated by author(s): May 15, 2019

Reporting Summary

Nature Research wishes to improve the reproducibility of the work that we publish. This form provides structure for consistency and transparency in reporting. For further information on Nature Research policies, see Authors & Referees and the Editorial Policy Checklist.

Statistics

For all statistical analyses, confirm that the following items are present in the figure legend, table legend, main text, or Methods section.

n/a	Confirmed	
☐	☒	The exact sample size (*n*) for each experimental group/condition, given as a discrete number and unit of measurement
☐	☒	A statement on whether measurements were taken from distinct samples or whether the same sample was measured repeatedly
☐	☒	The statistical test(s) used AND whether they are one- or two-sided *Only common tests should be described solely by name; describe more complex techniques in the Methods section.*
☒	☐	A description of all covariates tested
☐	☒	A description of any assumptions or corrections, such as tests of normality and adjustment for multiple comparisons
☐	☒	A full description of the statistical parameters including central tendency (e.g. means) or other basic estimates (e.g. regression coefficient) AND variation (e.g. standard deviation) or associated estimates of uncertainty (e.g. confidence intervals)
☐	☒	For null hypothesis testing, the test statistic (e.g. *F*, *t*, *r*) with confidence intervals, effect sizes, degrees of freedom and *P* value noted *Give P values as exact values whenever suitable.*
☒	☐	For Bayesian analysis, information on the choice of priors and Markov chain Monte Carlo settings
☒	☐	For hierarchical and complex designs, identification of the appropriate level for tests and full reporting of outcomes
☒	☐	Estimates of effect sizes (e.g. Cohen's *d*, Pearson's *r*), indicating how they were calculated

Our web collection on statistics for biologists contains articles on many of the points above.

Software and code

Policy information about availability of computer code

Data collection	*Provide a description of all commercial, open source and custom code used to collect the data in this study, specifying the version used OR state that no software was used.*
Data analysis	For flow cytometry software information, please see the flow cytometry form. All graphing and associated statistical analysis was performed using GraphPad Prism 7 or newer. MAVEN (build 682) was used for LC-MS analysis (http://genomics-pubs.princeton.edu/mzroll/index.php). STAR 2.7.0 was used for alignment of RNA-seq data. HTseq 0.11.1 was used for gene expression. DEseq2 was used for differential expression.

For manuscripts utilizing custom algorithms or software that are central to the research but not yet described in published literature, software must be made available to editors/reviewers. We strongly encourage code deposition in a community repository (e.g. GitHub). See the Nature Research guidelines for submitting code & software for further information.

Data

Policy information about availability of data

All manuscripts must include a data availability statement. This statement should provide the following information, where applicable:

- Accession codes, unique identifiers, or web links for publicly available datasets
- A list of figures that have associated raw data
- A description of any restrictions on data availability

The data that support the findings of this study are available from the corresponding author upon reasonable request. RNA-seq data sets have been deposited in Gene Expression Omnibus under the accession number GSE130713

Field-specific reporting

Please select the one below that is the best fit for your research. If you are not sure, read the appropriate sections before making your selection.

☒ Life sciences ☐ Behavioural & social sciences ☐ Ecological, evolutionary & environmental sciences

For a reference copy of the document with all sections, see nature.com/documents/nr-reporting-summary-flat.pdf

Life sciences study design

All studies must disclose on these points even when the disclosure is negative.

Sample size	No statistical methods were used to predetermine sample size for experimentation. Given the minimal experimental variation in T cell assays using inbred mouse strains as a cell source, a minimum of three technical replicates were used per sample.
Data exclusions	sgRNA transduction experiments were evaluated based on the efficacy of positive and negative controls. Experiments for which the positive or negative controls did not yield expected results were excluded. Predetermined exclusion criteria indicated that any experiment for which transduction with Tbx21 targeting sgRNA (experimental positive control) did not yield a significant ($p<0.05$) decrease in IFNg expression was to be excluded. No other data were excluded.
Replication	Using the data quality parameters described above, all experiments shown in the manuscript were reliably reproducible
Randomization	Because all cells used for analysis were from the same inbred strain of mouse, no randomization was performed.
Blinding	No blinding was performed. Blinding was unnecessary as all data collection and analysis is quantitative and not qualitative in nature.

Reporting for specific materials, systems and methods

We require information from authors about some types of materials, experimental systems and methods used in many studies. Here, indicate whether each material, system or method listed is relevant to your study. If you are not sure if a list item applies to your research, read the appropriate section before selecting a response.

Materials & experimental systems

n/a	Involved in the study
☐	☒ Antibodies
☐	☒ Eukaryotic cell lines
☒	☐ Palaeontology
☐	☒ Animals and other organisms
☒	☐ Human research participants
☒	☐ Clinical data

Methods

n/a	Involved in the study
☒	☐ ChIP-seq
☐	☒ Flow cytometry
☒	☐ MRI-based neuroimaging

Antibodies

Antibodies used	anti-CD4 Pe-Cy7 Biolegend Cat#100422 Clone#GK1.5 Lot#B224943 (1:1000) anti-Tbet e660 eBioscience Cat#50-5825-80 Clone#eBio4b10 Lot#e12135-1634 (1:50) anti-CD90.2 APC BD Cat#553007 Clone#53-2.1 Lot#72965 (1:500) Anti-Ifng BV421 Biolegend Cat#505829 Clone#XMG1.2 Lot#B214227 (1:400) Anti-Ifng e660 eBioscience Ref#50-7311-82 Clone#XMG1.2 Lot#e15675-103 (1:400) anti-GFP FITC Life Technologies Cat#A21311 Polyclonal Lot#1567217 (1:200) anti-mouse Ki-67 Biolegend Cat#652422 Clone 16A8 (1:200) anti-mouse H3 Cell Signaling Cat#14269S Clone 1B1B2 (1:200) anti-mouse Acetyl-histone H3(lys9) Cat#9649S Clone C5B11 (1:50) anti-mouse Acetyl-histone H3 (Lys27) Cat#8173S Clone D5E4 (1:50)
Validation	All antibodies listed have been used by a large number of laboratories including our own for many publications, including those in Nature. Each antibody is validated by the company of purchase, and dilution is determined experimentally for each clone individually.

Eukaryotic cell lines

Policy information about cell lines

Cell line source(s)	293T (ATCC CRL-3216)
Authentication	Cell lines obtained directly from ATCC. No cell line authentication performed.
Mycoplasma contamination	Cell lines were not tested for mycoplasma
Commonly misidentified lines (See ICLAC register)	The cell line used is not listed in the ICLAC database.

Animals and other organisms

Policy information about studies involving animals; ARRIVE guidelines recommended for reporting animal research

Laboratory animals	Mus musculus, B6, sex-matched male and female, 6-8 weeks old
Wild animals	n/a
Field-collected samples	n/a
Ethics oversight	All mice required for this study were housed and maintained under specific-pathogen-free conditions in the animal facility of the Yale University School of Medicine, and all corresponding animal protocols were approved by the Institutional Animal Care and Use Committee (IACUC) of Yale University. This study was conducted in compliance with all relevant ethical regulations.

Note that full information on the approval of the study protocol must also be provided in the manuscript.

Flow Cytometry

Plots

Confirm that:

☒ The axis labels state the marker and fluorochrome used (e.g. CD4-FITC).

☒ The axis scales are clearly visible. Include numbers along axes only for bottom left plot of group (a 'group' is an analysis of identical markers).

☒ All plots are contour plots with outliers or pseudocolor plots.

☒ A numerical value for number of cells or percentage (with statistics) is provided.

Methodology

Sample preparation	Cells were harvested, washed at least once with PBS, and stained with antibodies targeting surface antigens in 2%FBS 1mM EDTA in PBS for 30 minutes on ice. For analysis of intracellular cytokine staining, cells were then fixed and permeabilized with fixation/ permeabilization solution (BD Cytofix/Cytoperm Cat#554714) at 4C for 20 minutes. For nuclear transcription factor staining, cells were fixed and permeabilized with eBioscience Foxp3/Transcription Factor Fixation/Permeabilization Concentrate and Diluent (Cat #00-5521-00). Cells were then washed three times with 1X permeabilization buffer (eBioscience Permeabilization Buffer Cat #00-8333-56) and stained for intracellular antigens for 1 hour on ice in 1X permeabilization buffer. Cells were then washed two times before proceeding to cytometry analysis. For cells not transduced with retrovirus, cells were labeled with LIVE/DEAD Fixable Aqua Dead Cell Stain Kit (ThermoFisher Cat# L34965) per the manufactures protocol before surface staining. Further details regarding specific staining protocols and antibodies used can be found in the methods section of the manuscript. Cells were harvested, washed at least once with PBS, and stained with antibodies targeting surface antigens in 2%FBS 1mM EDTA in PBS for 30 minutes on ice. For analysis of intracellular cytokine staining, cells were then fixed and permeabilized with fixation/ permeabilization solution (BD Cytofix/Cytoperm Cat#554714) at 4C for 20 minutes. For nuclear transcription factor staining, cells were fixed and permeabilized with eBioscience Foxp3/Transcription Factor Fixation/Permeabilization Concentrate and Diluent (Cat #00-5521-00). Cells were then washed three times with 1X permeabilization buffer (eBioscience Permeabilization Buffer Cat #00-8333-56) and stained for intracellular antigens for 1 hour on ice in 1X permeabilization buffer. Cells were then washed two times before proceeding to cytometry analysis. For cells not transduced with retrovirus, cells were labeled with LIVE/DEAD Fixable Aqua Dead Cell Stain Kit (ThermoFisher Cat# L34965) per the manufactures protocol before surface staining. Further details regarding specific staining protocols and antibodies used can be found in the methods section of the manuscript.
Instrument	BD LSRII custom order product
Software	BD FACSDiva Software was used to collect raw data files from all flow cytometry experiments. All resultant data files were analyzed using FlowJo version 8 or newer.
Cell population abundance	Cells were purified for three replicate screens using a BD FACS Aria as described in methods. Due to limited cell numbers, all resultant cells were processed for gDNA isolation and sequencing.

Purity of magnetic bead CD4+ T cell isolation was determined by flow cytometry with >90% CD4 expressing cells used for all experiments.

Gating strategy

For all experiments measuring Ifng-Kat reporter expression, cells were gated on FSC-A high, DAPI low >> lymphocyte FSC-A, SSC-a >> CD4 positive, GFP positive based on clear distinctions between populations in the pseudo-color plot. Cells were binned into 4 quartiles of katushka expression. This gating strategy is shown in Extended Data Figure 4a.

For experiments measuring intracellular cytokine in retrovirally transduced cells, gating was as followed: FSC-A, SSC-A live cells >> SSC-W, SSC-H singlets >> FSC-H, FSC-W singlets >> CD4 positive, GFP positive live transduced cells.

For experiments measuring intracellular cytokine in cells not transduced, gating was as followed: FSC-A, SSC-A live cells >> SSC-W, SSC-H singlets >> FSC-H, FSC-W singlets >> CD4 positive, LIVE/DEAD Negative.

☒ Tick this box to confirm that a figure exemplifying the gating strategy is provided in the Supplementary Information.